Optical Lithography in the sub-50nm regime

Donis G. Flagello[a], Bill Arnold[a], Steve Hansen[a],
Mircea Dusa[b], Robert Socha[b],
Jan Mulkens[c], Rainer Garreis[d]

[a] ASML US, Inc., 8555 S. River Parkway, Tempe, Arizona, 85284
[b] ASML, 4800 Great America Parkway, Suite 400, Santa Clara, CA 95054
[c] ASML Netherlands B. V. , De Run 6501, 5504 DR Veldhoven, The Netherlands
[d] Carl Zeiss, D-73446 Oberkochen, Germany

ABSTRACT

The use of immersion technology will extend the lifetime of 193nm and 157nm lithography by enabling numerical apertures (NA) much greater than 1.0. A definition of effective k_1 is derived to assist in comparison of various technologies with differing optical characteristics. The ultimate limits of NA are explored by analysis of polarization effects at the reticle and imaging effects at the wafer. The effect of *Hertzian* or micro-polarization due to the size of the reticle structures is examined through rigorous simulation. For the regime of interest, 20nm to 50nm imaging, it is found that dense features on the reticle will polarize the light into the TE component upwards of 15%. Below this regime, the light becomes polarized in the TM direction. Additionally, oblique incidence on the reticle, resulting from large system NAs and 4x reduction, will cause PSM phase errors. The use of polarization in the illuminator for imaging will result in substantial gains in exposure latitude and MEF when the NA~1.3 with 45nm lines at 193nm. The end-of-line pullback for 2-dimensional patterns is reduced by the use of TE polarization in the illuminator. The overall polarization effects increase with decreasing k_1. The lower limit of optical lithography can be extended by using *source-mask* optimization and double exposure to go below the classical resolution limit, i.e., $k_1<0.25$.

Keywords: High NA, polarization, imaging, immersion, 193nm

1. INTRODUCTION

Optical lithography provides a high productivity, profitable means for making microcircuits on silicon wafers. By using higher and higher numerical apertures (NA), lower wavelengths, and resolution enhancement techniques (RETs) we have been able to push the limits of the optics well beyond would have been expected just a few years ago. Moving forward into the sub-50nm regime, we are faced with many new technology choices that are extremely complex and confound some of the typical scaling rule approximations.

The possible widespread use of immersion technology to enable hyper-NA systems (i.e., NA>1) will not only extend the lifetime of 193nm technology, but will delay the possible use of 157nm and EUV wavelengths. If one assumes that the maximum angle in the fluid medium should not extend beyond $\sin\theta=0.95$ using $\lambda=193$nm, then NAs up to ~1.35 can be contemplated when water is used as the immersion medium ($n_{water}=1.437$). However, if we also assume that higher index fluids ($n\geq1.6$) may be available, then the maximum NA could easily approach 1.5. Imaging at these NAs will require a fundamental understanding of the underlying optical phenomena associated with high angles, such as polarization behavior at reticle level, vector imaging effects at wafer level, and related effects within the optical systems.

The use of these NAs to extend imaging to sub-50nm levels will also require using a multitude of resolution enhancement techniques (RETs). One of the most powerful and complex RETs that will likely be needed to push the limitations of the optics is source-mask optimization[1]. This technique simultaneously optimizes the shape of the source and the reticle features to effectively solve the inverse imaging problem.

This paper will first show, in section 2, a method of comparing various optical imaging schemes, by introducing the definition of an effective k_1. For, example, this can be used to calculate the effective k_1 penalty using an unpolarized source over a TE polarized source. Section 3 will explore polarization effects due to the structure of a reticle. These

effects due to *Hertzian* polarization[2] can be significant and are dependent on the Cr thickness and angle of incidence. Section 4 will examine the vector effects in the image plane. The behaviors of 1-D and 2-D structures are analyzed and the impact of process window, mask error factor (MEF), and end-of-line (EOL) shortening are examined. Finally, section 5 looks at techniques to lower the half-pitch k_1 to <0.25 through the use of double expose techniques.

2. DEFINING *EFFECTIVE* k_1

A comparison of the various technologies is often difficult because of the widely differing illumination schemes, polarization conditions, reticle enhancements and processes. For example, polarization is not part of the resolution arguments, but at hyper-NA levels (i.e., NA>1.0) the imaging angles become large and the TM component of the electric field will lower will lower the image contrast, and hence, the effective k_1. By a careful analysis of the image on a film, we can derive an effective k_1 for any optical system. This will allow comparisons between different image approaches.

Let the image in a plane in a photoresist film be $I(r;z_0)$. Furthermore, the image is defined as a convolution of the object (mask) transmittance, $0(r)$, with a spread function, $H(r)$,

$$I(r;z_0) = O(r) \otimes H(r) \quad , \tag{1}$$

where r defines the image position in wafer coordinates. Now since the definitions of k_1 were originally based on the size and/or width of a point spread function defined by

$$PSF\left(r;\frac{NA}{\lambda}\right) = \left[\frac{2J_1\left(2\pi\frac{r\,NA}{\lambda}\right)}{\left(2\pi\frac{r\,NA}{\lambda}\right)}\right]^2 \quad , \tag{2}$$

where J_1 is the first-order Bessel function of the first kind. Since H(r)=PSF(r) for a perfectly incoherent system, by examining the parameter space of PSFs for various ratios of NA/λ, we can find a match to H(r) using a least-squares metric for any optical set-up and coherence. An effective k_1 can then be determined by

$$effective\ k_1 = CD \cdot \left(\frac{NA}{\lambda}\right)_{effective} \quad , \tag{3}$$

where the CD corresponds to the half pitch resolution.

Table I shows 5 different illumination and polarization configurations that were used to examine this technique for 45nm dense lines using water immersion at NA=1.3 and λ=193nm. The image at best focus (focus=0) and 0.2μm of defocus was simulated using Prolith™ software. Case 1 is used as a reference and uses a scalar calculation of the image in water with conventional circular illumination with a partial coherence filling of σ=1.0. All the other cases calculate the image at the top surface of a photoresist film of index, n=1.7-0.018i, on top of a matched substrate.

Table I: Illumination configurations to examine effective k_1

Case	*Simulation Model*	*Polarization Type*	*Illumination Configuration*
1	Scalar model in water	---	Circular, σ=1
2	Vector model in photoresist	Unpolarized	Annular, σ_{outer}=0.95, σ_{inner}=0.75
3	Vector model in photoresist	y oriented	Annular, σ_{outer}=0.95, σ_{inner}=0.75
4	Vector model in photoresist	Unpolarized	Dipole, σ_{center}=0.82, σ_{radius}=0.1
5	Vector model in photoresist	y oriented	Dipole, σ_{center}=0.82, σ_{radius}=0.1

Figure 1 shows the resulting effective k_1 for each case. According to the Rayleigh equation (i.e., resolution=k_1 x λ/NA), k_1=0.30 at this resolution. Case 1 is very close to this with k_1=0.31. The small difference with theory is probably due to numerical error within the simulator and fit routines and also to the fact that a truly incoherent source has σ=∞. Figure 2 shows the associated process windows for all the cases in photoresist. Unpolarized annular illumination produces

similar effective k_1 values as the reference. The corresponding process windows are small with low exposure latitude (EL) value of 5%. However the use of y polarization increases the process window and raises the effective k_1 by 35%. For dense lines in one direction the optimal illumination is a dipole. The effective k_1, as shown in figure 1 is now increased 58% to effective k_1=0.48. The use of polarization with this illumination increases the effective k_1 to 0.67 or a 116% increase over an unpolarized, annular illumination. Figure 2 shows the corresponding process window exhibiting substantial increase in exposure latitude and depth of focus.

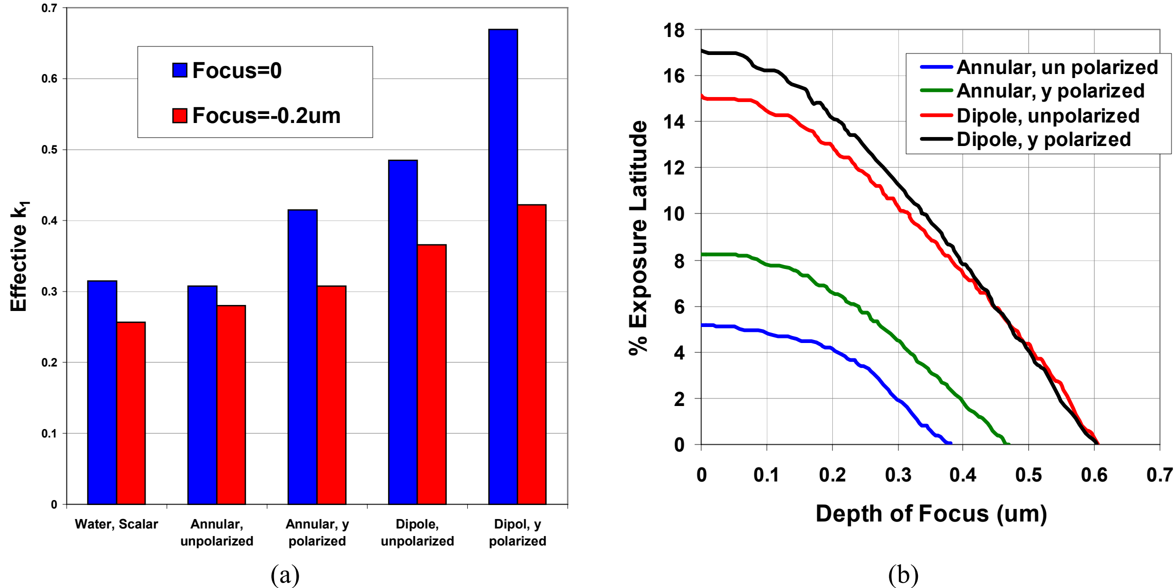

(a) (b)

Fig. 1. (a) Effective k_1 for 5 illumination and polarization configurations, (b) process windows for the configurations in photoresist. All simulations and calculations use λ=193nm with water immersion, NA=1.3, and 45nm dense lines.

3. HERTZIAN POLARIZATION DUE TO RETICLE FEATURES

The effect of *Hertzian* or micro-polarization due to the size of the reticle structures can be significant. This effect is especially strong considering that assist features for 193nm will be close to the actinic wavelength. Periodic structures can behave similar to wire-grids used to manufacture polarizers at longer wavelength regimes. The full impact at lithographic wavelengths will depend on the exact materials used in reticle fabrication and processing. The analysis is simplified here using Cr on quartz structures for the reticles, where the Cr index is n_{Cr}=0.84-1.65i, and the quartz is n_{quartz}=1.56.

The polarization effect can be analyzed using widely varying metrics. In this work, Panoramic Technologies software is used to simulate the near field transmission behavior of periodic features with 50% duty cycle, at an approximate distance of 2λ from the Cr. The transmission of the 0th order for TE and TM polarization is an indicator of the influence of feature size. For a system that does not induce polarization, this term will be unchanged for all feature sizes. Intensity is defined here as the magnitude of the time-averaged Poynting vector, and we define a polarization metric as the fraction of light that is TE polarized[3],

$$\text{Polarized Fraction} = \frac{I_{TE} - I_{unpolarized}}{I_{TE}} = \frac{I_{TE} - I_{TM}}{I_{TE} + I_{TM}} \quad . \tag{4}$$

Figure 3 shows the polarized fraction as a function of CD in wafer coordinates for 2 thicknesses of Cr. We see that between CD=5nm and 15nm the fraction is negative, indicating that the reticles are polarizing the light into the TM mode, which is perpendicular to the lines. This is classified as the *wire-grid zone*, and is consistent with theory that defines this zone when the reticle feature pitch < λ/2. Beyond this zone, the fractional polarization is positive indicating

that the reticle features polarize the light into the TE mode, which is parallel to the lines. This is considered as the *wave-guiding zone*. The existence of a peak between CD=20nm and 25nm is a indication of resonance and coincides with the reticle CD≈λ. We see that the light can be polarized up to 12% into the TE mode for the range between 32nm and 50nm. In practical terms, the lower limit of 32nm would be encountered with NA=1.5 and k_1=0.25 (cutoff).

Ideally having light that is strictly TE polarized would be the optimum, as this will help reduce image contrast loss due to vector effects[4]. Figure 3 would then imply that having a larger thickness is beneficial to the imaging. However, this must be weighted against the possible detrimental effects that thicker Cr will have on reticle processing and reticle CD uniformity. A more desired situation would be an extremely stable polarized illumination system that would largely eliminate the polarization contribution from the reticle. Also switching to a higher reduction ratio would lower the reticle's polarization effect. Figure 4 shows the decrease in polarization fraction for 32nm and 45nm feature sizes with increasing reduction using a Cr thickness of 110nm.

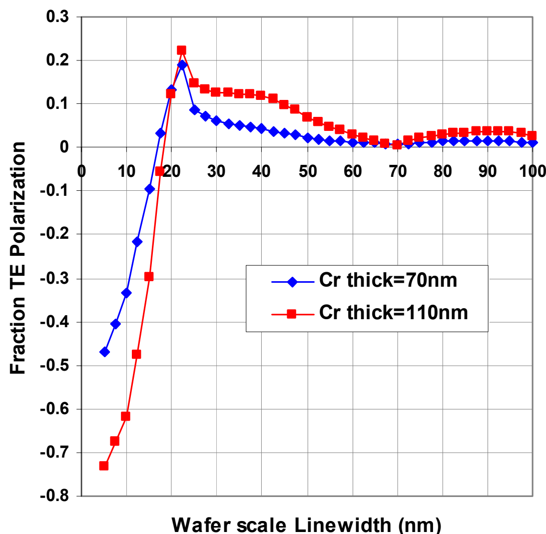

Fig. 3. Fraction of 0th order light that is TE polarized for 2 reticle Cr thicknesses as a function of line width. Reticle patterns are dense lines with 50% duty cycle.

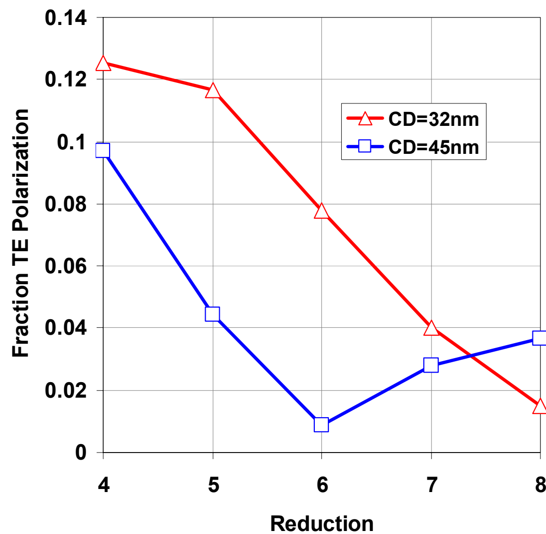

Fig. 4. Fraction of 0th order light that is TE polarized for 2 reticle dense line sizes (wafer scale) as a function of system reduction.

As the image-side NA increases substantially beyond 1, we also need to consider the impact of illumination angles impinging on the reticle. Since the system magnification can be defined by

$$m = \frac{1}{R} = \frac{NA_{object}}{NA_{image}} \quad , \tag{6}$$

where R is the reduction ratio, the maximum angle that will impinge on the reticle can vary substantially. Table II shows this angle with various NAs and reductions ratios, where the maximum angle is defined by the maximum illumination extent given by the partial coherence σ and can be written as

$$angle_{\max} = \frac{\sigma\, NA_{image}}{R} \quad . \tag{7}$$

Table II: Reticle side maximum angles (s=1) associated with various system NAs and reduction factors.

	NA=0.9	NA=1.0	NA=1.1	NA=1.2	NA=1.3	NA=1.4	NA=1.5	NA=1.6
4x	13	14	16	17	19	20	22	24
5x	10	12	13	14	15	16	17	19
6x	9	10	11	12	13	13	14	15
7x	7	8	9	10	11	12	12	13
8x	6	7	8	9	9	10	11	12

The 2 main effects of this varying incidence angle will be polarization and phase shifts induced by reticle features. Figure 5 shows the impact of angle on the previous Cr on quartz example. We see that there is almost no effect when the angles of incidence are between 0 and 10°. The fractional polarization increases slightly beyond this for the thinner Cr. The smaller line widths and thicker Cr have the larger amount of fractional polarization.

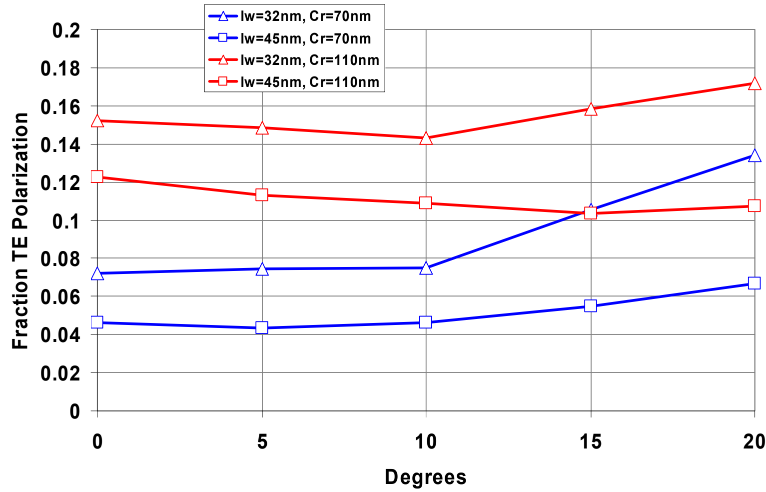

Fig. 5. Fraction of 0th order light that is TE polarized for 2 reticle dense line sizes (wafer scale) and Cr thickness as a function of incidence angle at the reticle.

The impact of illumination angle on phase masks is done by considering a simple phase mask geometry, as shown in figure 6. For normally incident rays the optical path difference (OPD) must be λ/2 for 180 phase mask and is given by

$$OPD_0 = n(D+d) - (nD+d) = d(n-1) = \frac{\lambda}{2} \quad . \tag{8}$$

This gives a solution for the quartz thickness difference of

$$d_0 = \frac{\lambda}{2(n-1)} \quad . \tag{9}$$

Now consider the situation where the incident rays are oblique. The OPD is then given by

$$OPD = \frac{n(D+d)}{\cos\theta'} - \left(\frac{nD}{\cos\theta'} + \frac{d}{\cos\theta}\right) = d\left(\frac{n}{\cos\theta'} - \frac{1}{\cos\theta}\right) = \frac{\lambda}{2} \quad , \tag{10}$$

and the required quartz thickness difference is

$$d = \frac{\lambda}{2\left(\frac{n}{\cos\theta'} - \frac{1}{\cos\theta}\right)} \quad . \tag{11}$$

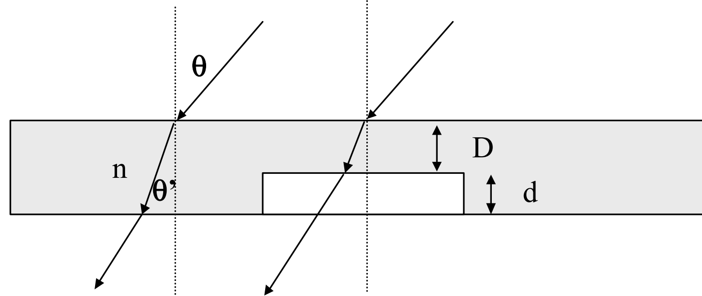

Fig. 6. Phase mask geometry with oblique angles of incidence.

If we substitute the quartz thickness assumed in equation (9) into equation (10) we can calculate a phase error that will be induced with high angles of incidence. Figure 7 shows a plot of the phase error in degrees. We have used the system NA as the maximum oblique angle. Clearly, the worst errors are for the highest illumination angles. It should be noted that while ordinary alternating phase mask use small σ and angles close to normal incidence, CPL type masks need to use off-axis illumination at large incidence angles. This implies that the specification of phase will depend on the specific RET solution and the number of distinct feature sizes. Additionally, we can see that the phase errors diminish with increasing reduction ratio. The implications of this are that the use of a higher reduction ratio may be beneficial in reducing the complexity of phase masks for hyper-NA systems.

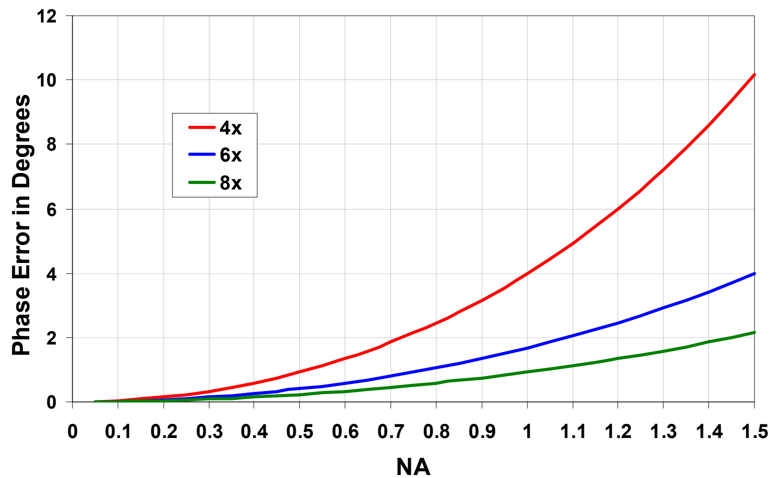

Fig. 7. Phase error as a function of the system numerical aperture associated with phase masks if the quartz depth is specified only at normal incidence.

4. HYPER-NA POLARIZATION EFFECTS

The effects and limits of hyper-NA imaging are explored by examining the impact of polarization on the imaging in a photoresist. This section first looks at the polarization effects on simple 1-D structures. This allows for the analysis and calculation of process windows and CD uniformity that is applicable to a large classification of general structures. However, some feature types will be more complex and require a more complex, 2-D analysis. This is done in the second half of the section with some preliminary analysis of process windows for line features with differing x-y periodicity and also end-of-line printing.

4.1. Simulation and Analysis of 1-D Features

Current optical systems are generally unpolarized. However, as the NA is increased, the influence of vector components on the imaging also increases. Specifically, the contribution of the TM polarization state results in a decrease in image contrast that tends to go as $\cos^2\theta$, where θ is the angle within the interfering medium. A classic example of this is coherent 2-wave imaging. This optically approximates specialized RETs such as dipole illumination and very small partial coherence for alternating phase shifting masks. If we let the angle in the resist for each wave be

$$\theta_{resist} = \sin^{-1}\frac{NA}{n_{resist}} \,, \tag{12}$$

and since the TE component contrast within a medium will always be 100%, the unpolarized contrast in the interference can be written as

$$Contrast_{resist} = \frac{1+\cos\left(2\theta_{resist}\right)}{2} \,. \tag{13}$$

Figure 8 shows a calculation of equation (13) using a wide range of real valued refractive indices and NAs. We have included the vacuum index as a reference, as well as, water. Since the refractive index for most photoresists is $n_{resist} \approx 1.7$, and if we accept a lower contrast limit of 0.4, we can image using an NA=1.3 with unpolarized illumination. However, if we require a higher, more conservative limit, such as 0.6, we will need to limit the quantity of TM polarization in the illumination beyond NA=1.1. If photoresist manufacturers can manage to increase the refractive index to close to 2.0, the NA limit range for unpolarized illumination moves up to NA=1.3-1.5. It is interesting to note that the contrast range in question, 0.4 to 0.6, pertains to $\sin\theta_{resist}$ = 0.65 – 0.75. The TM interference contrast goes exactly to 0 at $\sin\theta_{resist}$ =0.707 or θ_{resist} = 45°. The implications of this are that the key parameter for this image degradation is $\sin\theta_{resist}$, not necessarily NA. Hence, systems imaging in this angular range will probably require some form of polarization to compensate for polarization degradation, regardless of the NA.

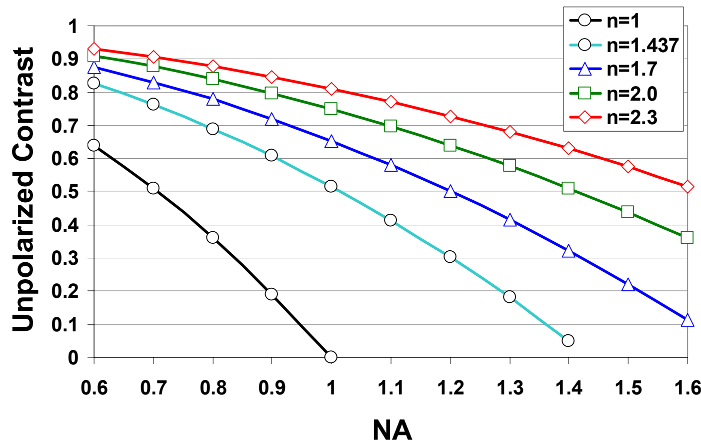

Fig. 8. Unpolarized image contrast as a function of system NA assuming 2-beam interference in a medium of refractive index, n.

In order to quantify the general impact of polarization on process windows for 193nm, simulations were done with dense and isolated lines. The dense lines used a binary mask, had a duty cycle of 50%, and used annular illumination with a partial coherent setting of σ_{outer}=0.95 an σ_{inner}=0.75. This condition is a typical off-axis illumination case that would be applied for many random feature types. The isolated lines used an alternating phase shift mask configuration where the pitch was set at 3.5 x CD with a circular illumination at σ=0.25. In order to accurately compare polarization effects the CDs are chosen at a constant k_1 value. In this fashion, the NAs can be compared to each other. Table III lists the NAs, k_1 values and associated CDs for this simulation.

Table III. Line sizes (nm) used for the simulations.

NA	k1	Iso Line CD	Dense Line CD	Pitch
1.05	0.3	55	31.4	109.9
1.05	0.325	60	34.3	120.05
1.05	0.35	64	36.6	128.1
1.1	0.3	53	30.3	106.05
1.1	0.325	57	32.6	114.1
1.1	0.35	61	34.9	122.15
1.15	0.3	50	28.6	100.1
1.15	0.325	55	31.4	109.9
1.15	0.35	59	33.7	117.95
1.2	0.3	48	27.6	96.5
1.2	0.325	52	29.9	104.5
1.2	0.35	56	32.2	112.6
1.25	0.3	46	26.3	92.05
1.25	0.325	50	28.6	100.1
1.25	0.35	54	30.9	108.15
1.3	0.3	45	25.7	89.95
1.3	0.325	48	27.4	95.9
1.3	0.35	52	29.7	103.95

The simulations were done using Prolith™ v8.0 with a calibrated 193nm-photoresist model with vector imaging. The film stack was restricted to 150nm of photoresist on a matched substrate with a complex index of n_{resist}=1.7-0.018i. The maximum depth of focus (DOF), exposure latitude (EL), and the mask error factor (MEF) were calculated for an NA range between 1.05 and 1.3 assuming water immersion lithography with n_{water}=1.437.

Figures 9a-c show the unpolarized exposure latitude, the maximum DOF and the mask error factor for the dense line cases. There is an overall degradation of all of these process metrics as the NA is increased and as the k_1 factor is decreased. The use of TE polarization, or polarization that is parallel to the line orientation, i.e. the y direction, increases the overall image contrast and process latitude. This is shown in figures 10a-c as the fraction improvement or gain when using a y-polarized source with dense lines. The improvement in EL and MEF are to be expected as they are proportional to the contrast; however, we note that DOF also increases, especially for k_1=0.3. In these cases, unpolarized illumination has a minimal process window, so that, if the general image contrast is increased, it results in an overall increase in all image metrics.

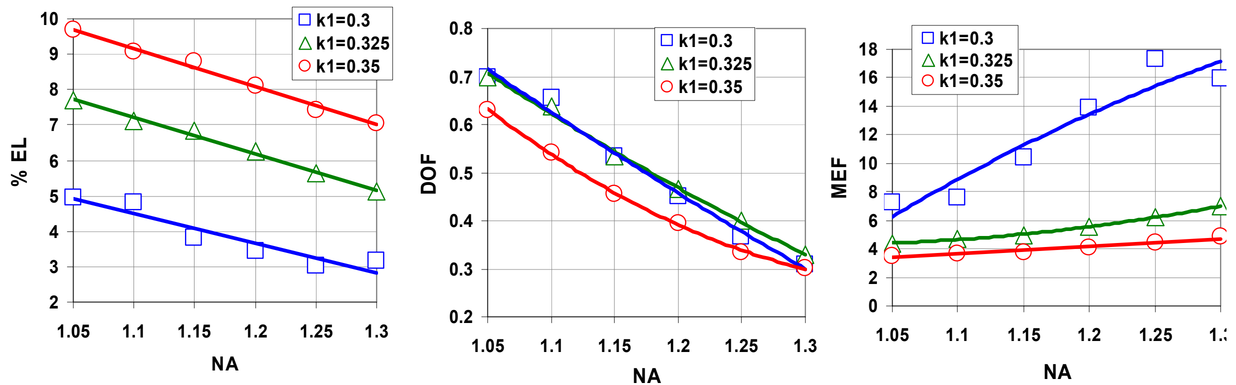

Fig. 9. Simulation results of the dense line case with unpolarized illumination.

There is an overall degradation of all of these process metrics as the NA is increased and as the k_1 factor is decreased. The use of TE polarization, or polarization that is parallel to the line orientation, i.e. the y direction, increases the overall image contrast and process latitude. This is shown in figures 10a-c as the fraction improvement or gain when using a y-

polarized source with dense lines. The improvement in EL and MEF are to be expected as they are proportional to the contrast; however, we note that DOF also increases, especially for k_1=0.3. In these cases, unpolarized illumination has a minimal process window, so that, if the general image contrast is increased, it results in an overall increase in all image metrics.

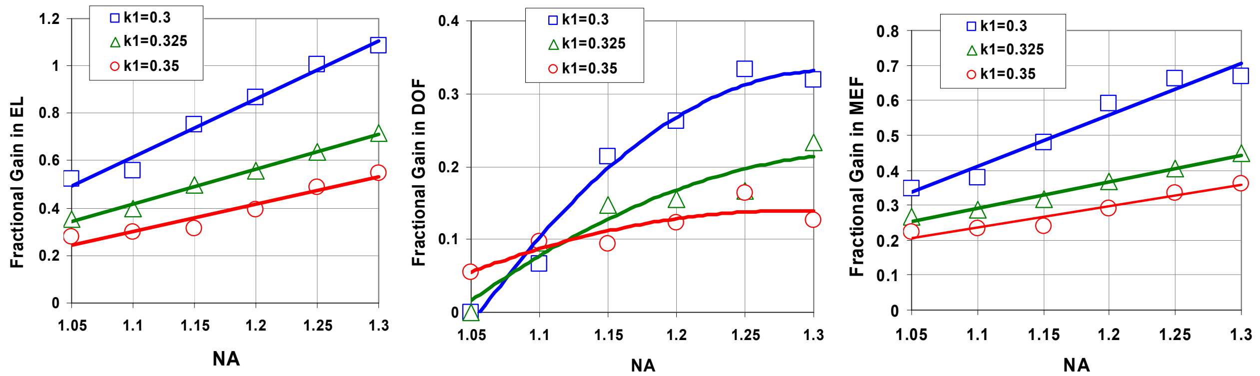

Fig. 10. Fractional gains in process window metrics when using a TE polarized illuminator.

In comparison to the dense case, figures 11 and 12 show the results for the alt-PSM. Although there is degradation for exposure latitude that scales with NA and k_1, the DOF and MEF have different behavior. The DOF is more or less independent of k_1 and the MEF, due to extremely low values for the unpolarized case. The improvement only occurs as the NA and k_1 values are at their maximum and minimum values, respectively. However, we note that the improvement in exposure latitude is very large, more than doubling at NA=1.15 and k_1=0.3 or CD=29nm.

The impact that polarization has on CD uniformity can be seen by using Monte Carlo techniques on the process window[5]. Using the isolated alt-PSM simulations, we calculated the CD uniformity for NA=1.3 for k_1=0.3. The results are given in figure 13 as contour plots and are a function of exposure variability and focus variability, both given as 3σ.

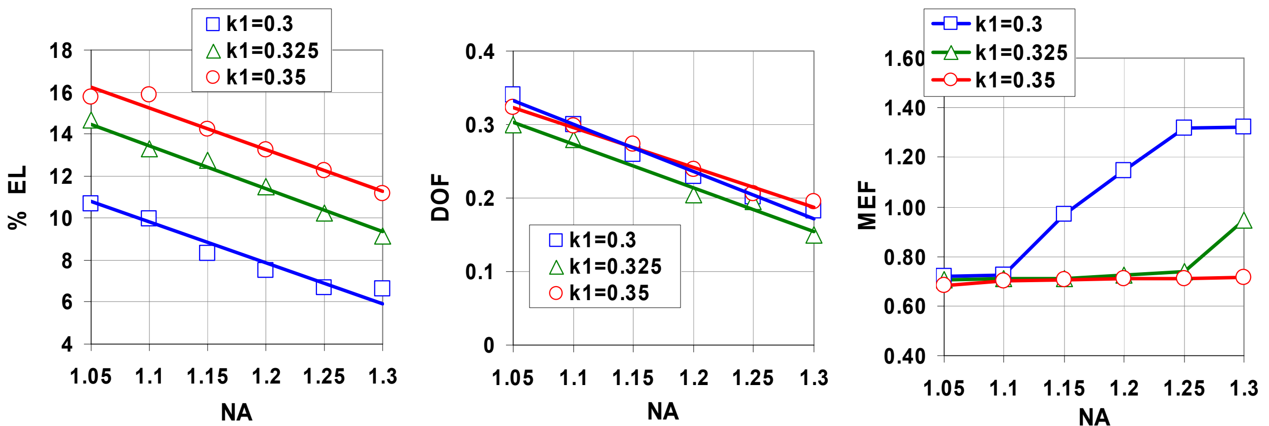

Fig. 11. Simulation results of the isolated line phase mask case with unpolarized illumination.

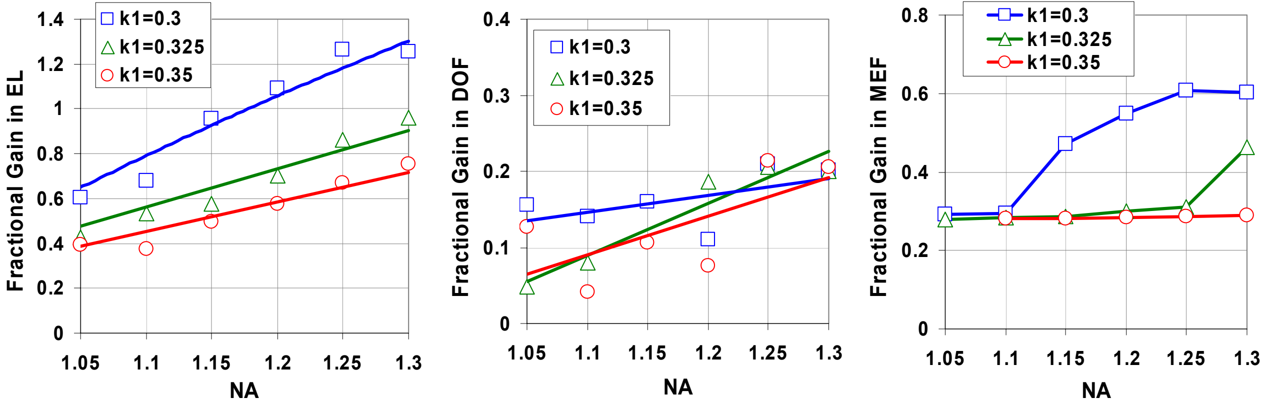

Fig. 12. Fractional gains in process window metrics when using a TE polarized illuminator.

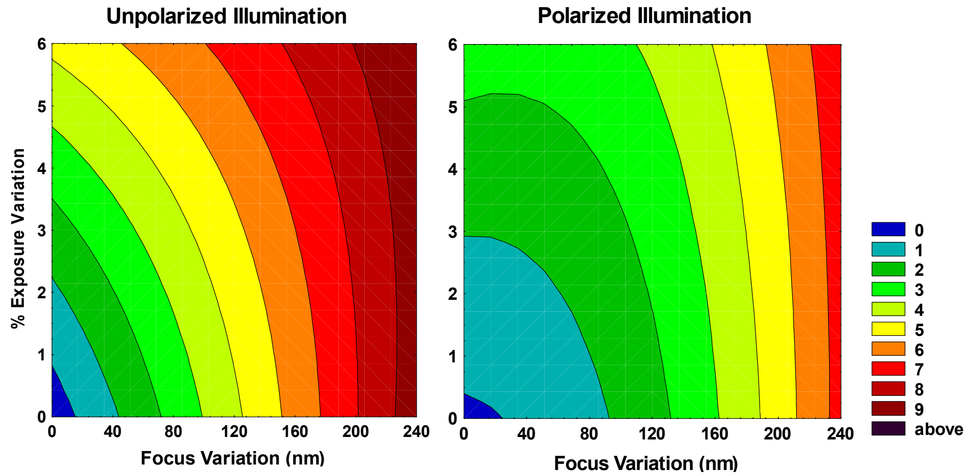

Fig. 13. 3σ CD uniformity (in nm) as a function of focus and exposure variation (also defined by 3σ) by Monte Carlo for isolated alt-PSM at k_1=0.3, NA=1.3, λ=193nm. Line size is 26nm on a 90nm pitch.

4.2. Simulation and Analysis of 2-D Features

Defining the best illumination polarization for 2-D features is much more complex than for simple 1-D line patterns. In the latter case, the term y-polarization is often used synonymously with TE polarization. In reality, y-polarization refers to a coordinate representation that is on the wafer, and TE polarization refers to a coordinate system in the lens pupil. Within the context of this paper, we define TE polarization (also known as azimuthal polarization) as being the direction of polarization that is tangential to the circle that defines the illumination pupil and TM polarization being perpendicular to that circle, or parallel to the radii of the pupil.

Since optical lithographic systems use and rely on partial coherence, the combination of illumination polarization, partial coherence, and complex 2-D structures will cause a mixing of polarization states that may not be easily visualized. This will be generally true unless there is a concerted effort made by the lithographer to orient his features to achieve the maximum benefit using polarized light.

Figure14 shows the image of a 45nm periodic line structure at the top surface of a photoresist n_{resist}=1.7 using a rigorous mask simulation and polarization using Panoramic™ software. The scalar, non-rigorous mask simulation is also shown. The NA=1.3 using annular illumination with σ_{outer}=0.95 and σ_{inner}=0.75. The pitch in the x direction is 90nm and the line lengths are 225nm. The pitch in the y direction is 292.5 giving the space between the line ends as 67.5nm. The

yellow contour is at the threshold that exactly defines the CD of the line in the x direction while the black contour shows the original mask. The end-of-line (EOL) pull back is quite strong for the TM polarization and is minimized using TE polarization. The TM and y polarization shows a large amount of structure deformation due to contrast loss in the direction parallel to the lines. We note that the x polarization does not behave exactly as TE polarization. The mixing of illumination and polarization produces a rounding of the line ends. Figure 15 gives the end-of-line pull back for all the conditions.

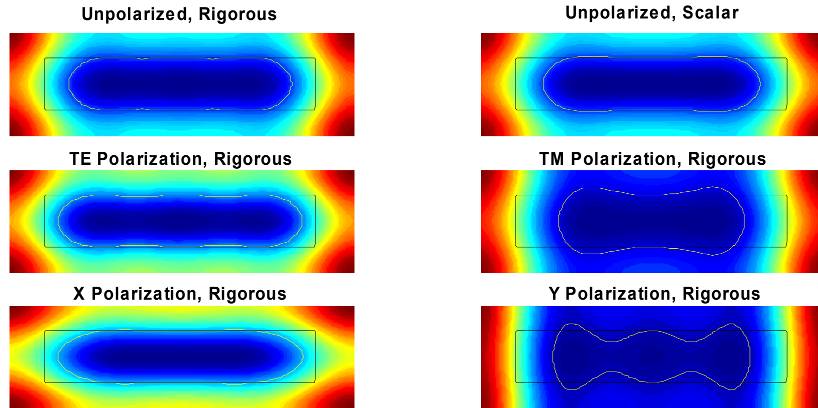

Fig.14. Images at the top surface of a photoresist for various polarization configurations.

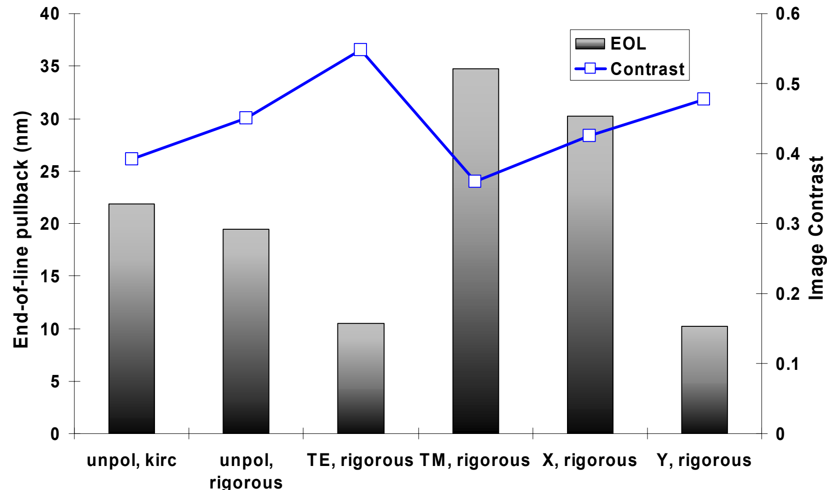

Fig. 15. EOL for images in fig.14 with associated image contrast

5. HOW FAR CAN WE EXTEND LITHOGRAPHY ?

The extension of 193nm to CDs below 45nm is possible if we assume that immersion lithography will be commercially successful and the industry will be able to increase the refractive index of the immersion fluid beyond that of pure water. However, the lower limit is still based on a physical limit of k_1=0.25 for optical imaging. The lower limit for manufacturing will probably be closer to k_1=0.3 because of the fall off in manufacturing yield as this hard barrier is approached.

One RET option that will have to be used is the *source-mask* optimization[1]. This technique is based on solving the inverse imaging equation by simultaneously deriving an optimized illumination and reticle for a given optical system. An example of this approach for a sub-50nm brick-wall feature using annular illumination is shown in figure 16a. This feature has a critical line width at 45nm with a 90nm pitch. The line length is 288nm with an end gap of 72nm. In best focus, at the nominal exposure, the annular illumination shows bulging line ends with a gap of 91.6nm or a 27.2% increase of the desired gap. Using an internal ASML algorithm, the optimum mask and illumination design can be calculated and are shown in figure 16b. The shape of the brick wall with the optimization routine is much closer to the desired shape. The gap now is 82.2nm or an increase in the gap of 14.2%. This is approximately a 2x improvement in the end-of-line.

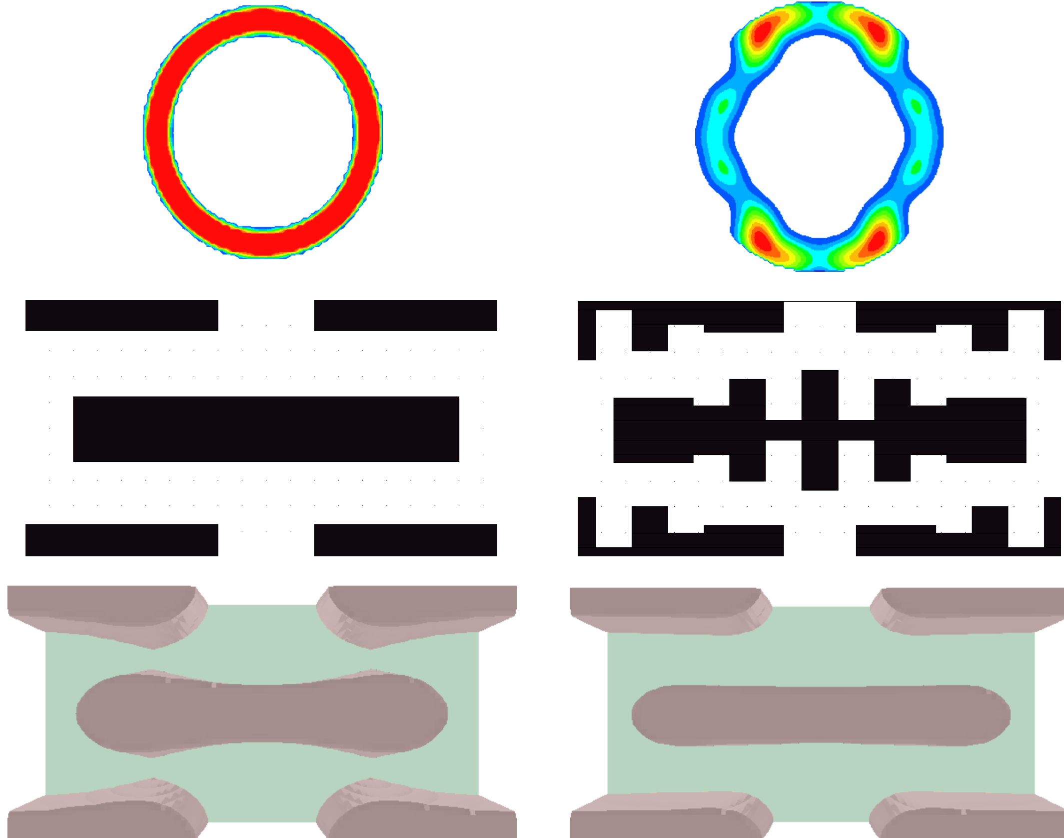

Fig. 16a. (Top) annular illumination source with souter=0.95 and sinner=0.75; (middle) traditional brick wall pattern; (bottom) resultant top-down photoresist pattern

Fig. 16 b. (Top) optimized illumination source; (middle) optimized brick wall pattern; (bottom) resultant top-down photoresist pattern

Assuming that we can arrive at a manufacturing process close to k_1=0.3 places a lower limit of 45nm (half-pitch) using NA=1.3. These limits may be overcome by the clever use of double exposure technology. Several double exposures or double processing schemes have been proposed in the past but many of these were designed to improve processing or clean up unwanted defects. A good example of this is the use of a trim mask exposure to remove unwanted artifacts in an alt-PSM gate process. Brueck[6] has proposed using double exposure techniques to go beyond the k_1=0.25 barrier by splitting the frequencies of the pattern. The intermediate developed photoresist is then etched to transfer the 1st intermediate image. Alternatively, each exposure can be done with 1 photoresist develop step, but this requires a fixation step to stabilize and threshold the 1st image such that it does not interact with the 2nd exposure.

The normal progression of meeting roadmap requirements by lowering wavelength to maintain reasonable k_1 values is meeting strong resistance due to cost of ownership issues. The necessary infrastructure that surrounds a new wavelength

includes significant reticle, pellicle, photoresist, and exposure tool development costs and risks. Double exposure technology has the possibility to enable the continuation of 193nm and 157nm lithography well beyond single exposure limitations. For example, let us assume that for 193nm each individual exposure is limited to a k_1=0.30. If advances in fluid materials will enable immersion fluids with an index >1.55, then we may be able to fabricate lenses with NA ≈ 1.5. This will allow us to do a half-pitch lithography of 20nm. A comparable double expose 157nm system would need NA=1.26 and a fluid index of 1.34. This is well within the realm of possibility to be developed for that time frame.

6. CONCLUSIONS AND REMARKS

Extension of optical lithography to the fabrication of integrated circuits with feature sizes less than 50nm has been examined. Hyper NA immersion projection optical systems coupled with polarized illumination sources offer an evolutionary path which takes full advantage of the highly successful infrastructure already built for reticles, pellicles, resists, and resolution enhancement techniques. Challenges in control of polarization effects, in maintaining sufficient depth of focus, and in minimization of mask error factor will continue to grow as NA increases and k_1 decreases. However, when these challenges are compared with those of new lithographic technologies, it is clear that silicon technologists will continue to look to extensions of optical lithography as the main approach for IC manufacturing for years to come.

7. REFERENCES

1. A. Rosenbluth et. al., “Optimum mask and source patterns to print a given shape”, *Proc. SPIE*, vol.4346, pp486-502 (2001)
2. T. Larsen, “A survey of the Theory of Wire Grids”, *IRE Transactions on Microwave Theory and Techniques*, 919-201 (May 1962)
3. M. Born and W. Wolf, *Principles of Optics*, Pergamon Press, Oxford, 1980
4. D. Flagello and A.E. Rosenbluth, “Lithographic tolerances based on vector diffraction theory”, J. Vac. Sci. Technol. B 10(6), 2997-3003 (1992)
5. K. Ronse et. al., “Characterization and Optimization of CD Control for 0.25µm C-MOS Applications”, *Proc. SPIE*, vol. 2726, 555, 1996
6. S. Brueck, “There are no fundamental limits to optical lithography”, *International Trends in Applied Optics*, A.H. Guenther, ed., SPIE Press (2002)